Measurements of Σ^+ and Σ^- time-like electromagnetic form factors for center-of-mass energies from 2.3864 to 3.0200 GeV

BESIII Collaboration [*]

M. Ablikim [a], M.N. Achasov [j,4], P. Adlarson [bs], S. Ahmed [o], M. Albrecht [d], A. Amoroso [bp,br], Q. An [bm,ax], Anita [u], Y. Bai [aw], O. Bakina [ae], R. Baldini Ferroli [w], I. Balossino [y], Y. Ban [an,12], K. Begzsuren [ab], J.V. Bennett [e], N. Berger [ad], M. Bertani [w], D. Bettoni [y], F. Bianchi [bp,br], J. Biernat [bs], J. Bloms [bj], A. Bortone [bp,br], I. Boyko [ae], R.A. Briere [e], H. Cai [bt], X. Cai [a,ax], A. Calcaterra [w], G.F. Cao [a,be], N. Cao [a,be], S.A. Cetin [bb], J.F. Chang [a,ax], W.L. Chang [a,be], G. Chelkov [ae,2,3], D.Y. Chen [f], G. Chen [a], H.S. Chen [a,be], M.L. Chen [a,ax], S.J. Chen [al], X.R. Chen [aa], Y.B. Chen [a,ax], W. Cheng [br], G. Cibinetto [y], F. Cossio [br], X.F. Cui [am], H.L. Dai [a,ax], J.P. Dai [ar,8], X.C. Dai [a,be], A. Dbeyssi [o], R.B. de Boer [d], D. Dedovich [ae], Z.Y. Deng [a], A. Denig [ad], I. Denysenko [ae], M. Destefanis [bp,br], F. De Mori [bp,br], Y. Ding [aj], C. Dong [am], J. Dong [a,ax], L.Y. Dong [a,be], M.Y. Dong [a,ax,be], S.X. Du [bw], J. Fang [a,ax], S.S. Fang [a,be], Y. Fang [a], R. Farinelli [y,z], L. Fava [bq,br], F. Feldbauer [d], G. Felici [w], C.Q. Feng [bm,ax], M. Fritsch [d], C.D. Fu [a], Y. Fu [a], X.L. Gao [bm,ax], Y. Gao [bn], Y. Gao [an,12], Y.G. Gao [f], I. Garzia [y,z], E.M. Gersabeck [bh], A. Gilman [bi], K. Goetzen [k], L. Gong [am], W.X. Gong [a,ax], W. Gradl [ad], M. Greco [bp,br], L.M. Gu [al], M.H. Gu [a,ax], S. Gu [b], Y.T. Gu [m], C.Y. Guan [a,be], A.Q. Guo [v], L.B. Guo [ak], R.P. Guo [ap], Y.P. Guo [ad], Y.P. Guo [i,9], A. Guskov [ae], S. Han [bt], T.T. Han [aq], T.Z. Han [i,9], X.Q. Hao [p], F.A. Harris [bf], K.L. He [a,be], F.H. Heinsius [d], T. Held [d], Y.K. Heng [a,ax,be], M. Himmelreich [k,7], T. Holtmann [d], Y.R. Hou [be], Z.L. Hou [a], H.M. Hu [a,be], J.F. Hu [ar,8], T. Hu [a,ax,be], Y. Hu [a], G.S. Huang [bm,ax], L.Q. Huang [bn], X.T. Huang [aq], Z. Huang [an,12], N. Huesken [bj], T. Hussain [bo], W. Ikegami Andersson [bs], W. Imoehl [v], M. Irshad [bm,ax], S. Jaeger [d], S. Janchiv [ab,11], Q. Ji [a], Q.P. Ji [p], X.B. Ji [a,be], X.L. Ji [a,ax], H.B. Jiang [aq], X.S. Jiang [a,ax,be], X.Y. Jiang [am], J.B. Jiao [aq], Z. Jiao [r], S. Jin [al], Y. Jin [bg], T. Johansson [bs], N. Kalantar-Nayestanaki [ag], X.S. Kang [aj], R. Kappert [ag], M. Kavatsyuk [ag], B.C. Ke [as,a], I.K. Keshk [d], A. Khoukaz [bj], P. Kiese [ad], R. Kiuchi [a], R. Kliemt [k], L. Koch [af], O.B. Kolcu [bb,6], B. Kopf [d], M. Kuemmel [d], M. Kuessner [d], A. Kupsc [bs], M.G. Kurth [a,be], W. Kühn [af], J.J. Lane [bh], J.S. Lange [af], P. Larin [o], L. Lavezzi [br], H. Leithoff [ad],

[*] E-mail address: besiii-publications@ihep.ac.cn.
[1] Also at Bogazici University, 34342 Istanbul, Turkey.
[2] Also at the Moscow Institute of Physics and Technology, Moscow 141700, Russia.
[3] Also at the Functional Electronics Laboratory, Tomsk State University, Tomsk, 634050, Russia.
[4] Also at the Novosibirsk State University, Novosibirsk, 630090, Russia.
[5] Also at the NRC "Kurchatov Institute", PNPI, 188300, Gatchina, Russia.
[6] Also at Istanbul Arel University, 34295 Istanbul, Turkey.
[7] Also at Goethe University Frankfurt, 60323 Frankfurt am Main, Germany.
[8] Also at Key Laboratory for Particle Physics, Astrophysics and Cosmology, Ministry of Education; Shanghai Key Laboratory for Particle Physics and Cosmology; Institute of Nuclear and Particle Physics, Shanghai 200240, People's Republic of China.
[9] Also at Key Laboratory of Nuclear Physics and Ion-beam Application (MOE) and Institute of Modern Physics, Fudan University, Shanghai 200443, People's Republic of China.
[10] Also at Harvard University, Department of Physics, Cambridge, MA, 02138, USA.
[11] Currently at: Institute of Physics and Technology, Peace Ave.54B, Ulaanbaatar 13330, Mongolia.
[12] Also at State Key Laboratory of Nuclear Physics and Technology, Peking University, Beijing 100871, People's Republic of China.
[13] School of Physics and Electronics, Hunan University, Changsha 410082, China.

M. Lellmann [ad], T. Lenz [ad], C. Li [ao], C.H. Li [ai], Cheng Li [bm,ax], D.M. Li [bw], F. Li [a,ax], G. Li [a], H.B. Li [a,be], H.J. Li [i,9], J.L. Li [aq], J.Q. Li [d], Ke Li [a], L.K. Li [a], Lei Li [c], P.L. Li [bm,ax], P.R. Li [ah], S.Y. Li [az], W.D. Li [a,be], W.G. Li [a], X.H. Li [bm,ax], X.L. Li [aq], Z.B. Li [ay], Z.Y. Li [ay], H. Liang [bm,ax], H. Liang [a,be], Y.F. Liang [au], Y.T. Liang [aa], L.Z. Liao [a,be], J. Libby [u], C.X. Lin [ay], B. Liu [ar,8], B.J. Liu [a], C.X. Liu [a], D. Liu [bm,ax], D.Y. Liu [ar,8], F.H. Liu [at], Fang Liu [a], Feng Liu [f], H.B. Liu [m], H.M. Liu [a,be], Huanhuan Liu [a], Huihui Liu [q], J.B. Liu [bm,ax], J.Y. Liu [a,be], K. Liu [a], K.Y. Liu [aj], Ke Liu [f], L. Liu [bm,ax], Q. Liu [be], S.B. Liu [bm,ax], Shuai Liu [av], T. Liu [a,be], X. Liu [ah], Y.B. Liu [am], Z.A. Liu [a,ax,be], Z.Q. Liu [aq], Y.F. Long [an,12], X.C. Lou [a,ax,be], F.X. Lu [p], H.J. Lu [r], J.D. Lu [a,be], J.G. Lu [a,ax], X.L. Lu [a], Y. Lu [a], Y.P. Lu [a,ax], C.L. Luo [ak], M.X. Luo [bv], P.W. Luo [ay], T. Luo [i,9], X.L. Luo [a,ax], S. Lusso [br], X.R. Lyu [be], F.C. Ma [aj], H.L. Ma [a], L.L. Ma [aq], M.M. Ma [a,be], Q.M. Ma [a], R.Q. Ma [a,be], R.T. Ma [be], X.N. Ma [am], X.X. Ma [a,be], X.Y. Ma [a,ax], Y.M. Ma [aq], F.E. Maas [o], M. Maggiora [bp,br], S. Maldaner [ad], S. Malde [bk], Q.A. Malik [bo], A. Mangoni [x], Y.J. Mao [an,12], Z.P. Mao [a], S. Marcello [bp,br], Z.X. Meng [bg], J.G. Messchendorp [ag], G. Mezzadri [y], T.J. Min [al], R.E. Mitchell [v], X.H. Mo [a,ax,be], Y.J. Mo [f], N.Yu. Muchnoi [j,4], H. Muramatsu [bi], S. Nakhoul [k,7], Y. Nefedov [ae], F. Nerling [k,7], I.B. Nikolaev [j,4], Z. Ning [a,ax], S. Nisar [h,10], S.L. Olsen [be], Q. Ouyang [a,ax,be], S. Pacetti [x], X. Pan [av], Y. Pan [bh], A. Pathak [a], P. Patteri [w], M. Pelizaeus [d], H.P. Peng [bm,ax], K. Peters [k,7], J. Pettersson [bs], J.L. Ping [ak], R.G. Ping [a,be], A. Pitka [d], R. Poling [bi], V. Prasad [bm,ax], H. Qi [bm,ax], H.R. Qi [az], M. Qi [al], T.Y. Qi [b], S. Qian [a,ax], W.-B. Qian [be], Z. Qian [ay], C.F. Qiao [be], L.Q. Qin [l], X.P. Qin [m], X.S. Qin [d], Z.H. Qin [a,ax], J.F. Qiu [a], S.Q. Qu [am], K.H. Rashid [bo], K. Ravindran [u], C.F. Redmer [ad], A. Rivetti [br], V. Rodin [ag], M. Rolo [br], G. Rong [a,be], Ch. Rosner [o], M. Rump [bj], A. Sarantsev [ae,5], M. Savrié [z], Y. Schelhaas [ad], C. Schnier [d], K. Schoenning [bs], D.C. Shan [av], W. Shan [s], X.Y. Shan [bm,ax], M. Shao [bm,ax], C.P. Shen [b], P.X. Shen [am], X.Y. Shen [a,be], H.C. Shi [bm,ax], R.S. Shi [a,be], X. Shi [a,ax], X.D. Shi [bm,ax], J.J. Song [aq], Q.Q. Song [bm,ax], W.M. Song [ac], Y.X. Song [an,12], S. Sosio [bp,br], S. Spataro [bp,br], F.F. Sui [aq], G.X. Sun [a], J.F. Sun [p], L. Sun [bt], S.S. Sun [a,be], T. Sun [a,be], W.Y. Sun [ak], Y.J. Sun [bm,ax], Y.K. Sun [bm,ax], Y.Z. Sun [a], Z.T. Sun [a], Y.H. Tan [bt], Y.X. Tan [bm,ax], C.J. Tang [au], G.Y. Tang [a], J. Tang [ay], V. Thoren [bs], B. Tsednee [ab], I. Uman [bd], B. Wang [a], B.L. Wang [be], C.W. Wang [al], D.Y. Wang [an,12], H.P. Wang [a,be], K. Wang [a,ax], L.L. Wang [a], M. Wang [aq], M.Z. Wang [an,12], Meng Wang [a,be], W.H. Wang [bt], W.P. Wang [bm,ax], X. Wang [an,12], X.F. Wang [ah], X.L. Wang [i,9], Y. Wang [bm,ax], Y. Wang [ay], Y.D. Wang [o], Y.F. Wang [a,ax,be], Y.Q. Wang [a], Z. Wang [a,ax], Z.Y. Wang [a], Ziyi Wang [be], Zongyuan Wang [a,be], T. Weber [d], D.H. Wei [l], P. Weidenkaff [ad], F. Weidner [bj], S.P. Wen [a], D.J. White [bh], U. Wiedner [d], G. Wilkinson [bk], M. Wolke [bs], L. Wollenberg [d], J.F. Wu [a,be], L.H. Wu [a], L.J. Wu [a,be], X. Wu [i,9], Z. Wu [a,ax], L. Xia [bm,ax], H. Xiao [i,9], S.Y. Xiao [a], Y.J. Xiao [a,be], Z.J. Xiao [ak], X.H. Xie [an,12], Y.G. Xie [a,ax], Y.H. Xie [f], T.Y. Xing [a,be], X.A. Xiong [a,be], G.F. Xu [a], J.J. Xu [al], Q.J. Xu [n], W. Xu [a,be], X.P. Xu [av], L. Yan [i,9], L. Yan [bp,br], W.B. Yan [bm,ax], W.C. Yan [bw], Xu Yan [av], H.J. Yang [ar,8], H.X. Yang [a], L. Yang [bt], R.X. Yang [bm,ax], S.L. Yang [a,be], Y.H. Yang [al], Y.X. Yang [l], Yifan Yang [a,be], Zhi Yang [aa], M. Ye [a,ax], M.H. Ye [g], J.H. Yin [a], Z.Y. You [ay], B.X. Yu [a,ax,be], C.X. Yu [am], G. Yu [a,be], J.S. Yu [t,13], T. Yu [bn], C.Z. Yuan [a,be], W. Yuan [bp,br], X.Q. Yuan [an,12], Y. Yuan [a], Z.Y. Yuan [ay], C.X. Yue [ai], A. Yuncu [bb,1], A.A. Zafar [bo], Y. Zeng [t,13], B.X. Zhang [a], Guangyi Zhang [p], H.H. Zhang [ay], H.Y. Zhang [a,ax], J.L. Zhang [bu], J.Q. Zhang [d], J.W. Zhang [a,ax,be], J.Y. Zhang [a], J.Z. Zhang [a,be], Jianyu Zhang [a,be], Jiawei Zhang [a,be], L. Zhang [a], Lei Zhang [al], S. Zhang [ay], S.F. Zhang [al], T.J. Zhang [ar,8], X.Y. Zhang [aq], Y. Zhang [bk], Y.H. Zhang [a,ax], Y.T. Zhang [bm,ax], Yan Zhang [bm,ax], Yao Zhang [a], Yi Zhang [i,9], Z.H. Zhang [f], Z.Y. Zhang [bt], G. Zhao [a], J. Zhao [ai], J.Y. Zhao [a,be], J.Z. Zhao [a,ax], Lei Zhao [bm,ax], Ling Zhao [a], M.G. Zhao [am], Q. Zhao [a], S.J. Zhao [bw], Y.B. Zhao [a,ax], Y.X. Zhao Zhao [aa], Z.G. Zhao [bm,ax], A. Zhemchugov [ae,2], B. Zheng [bn], J.P. Zheng [a,ax], Y. Zheng [an,12], Y.H. Zheng [be], B. Zhong [ak], C. Zhong [bn], L.P. Zhou [a,be], Q. Zhou [a,be], X. Zhou [bt], X.K. Zhou [be], X.R. Zhou [bm,ax], A.N. Zhu [a,be], J. Zhu [am], K. Zhu [a], K.J. Zhu [a,ax,be], S.H. Zhu [bl], W.J. Zhu [am], X.L. Zhu [az], Y.C. Zhu [bm,ax], Z.A. Zhu [a,be], B.S. Zou [a], J.H. Zou [a]

[a] *Institute of High Energy Physics, Beijing 100049, People's Republic of China*
[b] *Beihang University, Beijing 100191, People's Republic of China*
[c] *Beijing Institute of Petrochemical Technology, Beijing 102617, People's Republic of China*
[d] *Bochum Ruhr-University, D-44780 Bochum, Germany*
[e] *Carnegie Mellon University, Pittsburgh, PA 15213, USA*

[f] *Central China Normal University, Wuhan 430079, People's Republic of China*
[g] *China Center of Advanced Science and Technology, Beijing 100190, People's Republic of China*
[h] *COMSATS University Islamabad, Lahore Campus, Defence Road, Off Raiwind Road, 54000 Lahore, Pakistan*
[i] *Fudan University, Shanghai 200443, People's Republic of China*
[j] *G.I. Budker Institute of Nuclear Physics SB RAS (BINP), Novosibirsk 630090, Russia*
[k] *GSI Helmholtzcentre for Heavy Ion Research GmbH, D-64291 Darmstadt, Germany*
[l] *Guangxi Normal University, Guilin 541004, People's Republic of China*
[m] *Guangxi University, Nanning 530004, People's Republic of China*
[n] *Hangzhou Normal University, Hangzhou 310036, People's Republic of China*
[o] *Helmholtz Institute Mainz, Johann-Joachim-Becher-Weg 45, D-55099 Mainz, Germany*
[p] *Henan Normal University, Xinxiang 453007, People's Republic of China*
[q] *Henan University of Science and Technology, Luoyang 471003, People's Republic of China*
[r] *Huangshan College, Huangshan 245000, People's Republic of China*
[s] *Hunan Normal University, Changsha 410081, People's Republic of China*
[t] *Hunan University, Changsha 410082, People's Republic of China*
[u] *Indian Institute of Technology Madras, Chennai 600036, India*
[v] *Indiana University, Bloomington, IN 47405, USA*
[w] *INFN Laboratori Nazionali di Frascati, I-00044, Frascati, Italy*
[x] *INFN and University of Perugia, I-06100, Perugia, Italy*
[y] *INFN Sezione di Ferrara, I-44122, Ferrara, Italy*
[z] *University of Ferrara, I-44122, Ferrara, Italy*
[aa] *Institute of Modern Physics, Lanzhou 730000, People's Republic of China*
[ab] *Institute of Physics and Technology, Peace Ave. 54B, Ulaanbaatar 13330, Mongolia*
[ac] *Jilin University, Changchun 130012, People's Republic of China*
[ad] *Johannes Gutenberg University of Mainz, Johann-Joachim-Becher-Weg 45, D-55099 Mainz, Germany*
[ae] *Joint Institute for Nuclear Research, 141980 Dubna, Moscow region, Russia*
[af] *Justus-Liebig-Universitaet Giessen, II. Physikalisches Institut, Heinrich-Buff-Ring 16, D-35392 Giessen, Germany*
[ag] *KVI-CART, University of Groningen, NL-9747 AA Groningen, the Netherlands*
[ah] *Lanzhou University, Lanzhou 730000, People's Republic of China*
[ai] *Liaoning Normal University, Dalian 116029, People's Republic of China*
[aj] *Liaoning University, Shenyang 110036, People's Republic of China*
[ak] *Nanjing Normal University, Nanjing 210023, People's Republic of China*
[al] *Nanjing University, Nanjing 210093, People's Republic of China*
[am] *Nankai University, Tianjin 300071, People's Republic of China*
[an] *Peking University, Beijing 100871, People's Republic of China*
[ao] *Qufu Normal University, Qufu 273165, People's Republic of China*
[ap] *Shandong Normal University, Jinan 250014, People's Republic of China*
[aq] *Shandong University, Jinan 250100, People's Republic of China*
[ar] *Shanghai Jiao Tong University, Shanghai 200240, People's Republic of China*
[as] *Shanxi Normal University, Linfen 041004, People's Republic of China*
[at] *Shanxi University, Taiyuan 030006, People's Republic of China*
[au] *Sichuan University, Chengdu 610064, People's Republic of China*
[av] *Soochow University, Suzhou 215006, People's Republic of China*
[aw] *Southeast University, Nanjing 211100, People's Republic of China*
[ax] *State Key Laboratory of Particle Detection and Electronics, Beijing 100049, Hefei 230026, People's Republic of China*
[ay] *Sun Yat-Sen University, Guangzhou 510275, People's Republic of China*
[az] *Tsinghua University, Beijing 100084, People's Republic of China*
[ba] *Ankara University, 06100 Tandogan, Ankara, Turkey*
[bb] *Istanbul Bilgi University, 34060 Eyup, Istanbul, Turkey*
[bc] *Uludag University, 16059 Bursa, Turkey*
[bd] *Near East University, Nicosia, North Cyprus, Mersin 10, Turkey*
[be] *University of Chinese Academy of Sciences, Beijing 100049, People's Republic of China*
[bf] *University of Hawaii, Honolulu, HI 96822, USA*
[bg] *University of Jinan, Jinan 250022, People's Republic of China*
[bh] *University of Manchester, Oxford Road, Manchester, M13 9PL, UK*
[bi] *University of Minnesota, Minneapolis, MN 55455, USA*
[bj] *University of Muenster, Wilhelm-Klemm-Str. 9, 48149 Muenster, Germany*
[bk] *University of Oxford, Keble Rd, Oxford, OX13RH, UK*
[bl] *University of Science and Technology Liaoning, Anshan 114051, People's Republic of China*
[bm] *University of Science and Technology of China, Hefei 230026, People's Republic of China*
[bn] *University of South China, Hengyang 421001, People's Republic of China*
[bo] *University of the Punjab, Lahore-54590, Pakistan*
[bp] *University of Turin, I-10125, Turin, Italy*
[bq] *University of Eastern Piedmont, I-15121, Alessandria, Italy*
[br] *INFN, I-10125, Turin, Italy*
[bs] *Uppsala University, Box 516, SE-75120 Uppsala, Sweden*
[bt] *Wuhan University, Wuhan 430072, People's Republic of China*
[bu] *Xinyang Normal University, Xinyang 464000, People's Republic of China*
[bv] *Zhejiang University, Hangzhou 310027, People's Republic of China*
[bw] *Zhengzhou University, Zhengzhou 450001, People's Republic of China*

ARTICLE INFO

ABSTRACT

The Born cross sections of the $e^+e^- \rightarrow \Sigma^+\bar{\Sigma}^-$ and $e^+e^- \rightarrow \Sigma^-\bar{\Sigma}^+$ processes are determined for center-of-mass energy from 2.3864 to 3.0200 GeV with the BESIII detector. The cross section lineshapes can be described properly by a pQCD function and the resulting ratio of effective form factors for the Σ^+ and Σ^- is consistent with 3. In addition, ratios of the Σ^+ electric and magnetic form factors, $|G_E/G_M|$, are obtained at three center-of-mass energies through an analysis of the angular distributions.

These measurements, which are studied for the first time in the off-resonance region, provide precision experimental input for understanding baryonic structure. The observed new features of the $\Sigma^{\pm}$ form factors require more theoretical discussions for the hyperons.

1. Introduction

Nucleons, as the lightest baryons, are the largest component of the observable matter in the universe, and were shown to be non-pointlike particles in the middle of last century [1,2]. However, nucleon properties, such as their radii and the sources of their spin, are still not well understood [3]. The hyperons are the $SU(3)$-flavor-octet partners of the nucleons that contain one or more strange quarks, and offer crucial additional dimensions to the study of nucleon structures [4,5]. Treating the heavier strange quarks as spectators, hyperons can provide valuable insight into the behavior of the lighter up and down quarks in different environments. Electromagnetic form factors (EMFFs) are fundamental observables of baryons that are intimately related to their internal structure and dynamics [6–8]. Despite the fact that much work has been done on the EM structures of protons in both the space-like and time-like regions [9–14], experimental information regarding the EMFFs of hyperons remains limited [15–18]. Moreover, the few existing measurements of time-like neutron FFs [19,20] differ from each other and lead to conflicting conclusions when compared to those for the proton [21,22]. A Σ^+ hyperon is formed by replacing the proton's down quark with a strange quark; likewise a Σ^- is formed by replacing the neutron's up quark with a strange quark. The corresponding ratio of FFs between the Σ^+ and Σ^- hyperons could provide guidance for the nucleons. Therefore, experimental measurements for Σ hyperons, especially the Σ^-, which has never been measured in the time-like region, provide essential tests of various theoretical models [22–24] and produce important input for the understanding of baryonic structures.

The differential, one-photon exchange cross section for the $e^+e^- \to B\bar{B}$ process, where B is a spin-1/2 baryon, can be expressed in terms of the electric and magnetic FFs G_E and G_M as [25]:

$$\frac{d\sigma^B(s)}{d\Omega} = \frac{\alpha^2 \beta C |G_M|^2}{4s}\left[(1+\cos^2\theta) + \frac{1}{\tau}\left|\frac{G_E}{G_M}\right|^2 \sin^2\theta \right], \quad (1)$$

where α is the fine-structure constant, s is the square of center-of-mass (c.m.) energy, $\beta = \sqrt{1 - 4m_B^2/s}$ is a phase-space factor, $\tau = \frac{s}{4m_B^2}$, m_B is the baryon mass, and θ is its c.m. production angle. The Coulomb correction factor C [26,27] accounts for the electromagnetic interaction of charged point-like fermion pairs in the final state. It reads $C = y/(1 - e^{-y})$ with $y = \pi\alpha(1+\beta^2)/\beta$ for a charged point-like fermion pair and $C = 1$ for a neutral point-like fermion pair. For charged point-like fermion pairs, the cross section at threshold is non-zero, $\sigma(4m_B^2) = \pi^2\alpha^3/2m_B^2 = 848(m_p/m_B)^2$ pb, where m_p is the proton mass [28], and then grows with increasing β. Experimentally, a rapid rise of the $e^+e^- \to p\bar{p}$ cross section near threshold followed by a plateau is observed [12,13]. The cross section of plateau near threshold is consistent with the 848 pb expectation for a point-like charged particle. However, in this case, the $p\bar{p}$ is produced by a virtual photon with $Q^2 = 4m_p^2 = 3.53$ GeV², which corresponds to a Compton wavelength of ~0.1 fm, a scale at which the proton is definitely not point-like. A similar feature of the cross section for $e^+e^- \to \Lambda_c^+\bar{\Lambda}_c^-$ is observed by the BESIII experiment [29], where the cross section of plateau near threshold is around 240 pb. This is 1.6 times the predicted value for point-like charged particles. These unexpected threshold

effects have been widely discussed in the literature where they are interpreted as final state interactions [30], bound states or near-threshold meson resonances [31], or an attractive Coulomb interaction [32]. To understand the nature of these threshold effects, experimental measurements of the near threshold charged pair production of other hyperons will be of critical importance.

2. Detector and data sample

In this Letter, we present precision measurements of $e^+e^- \to \Sigma^+\bar{\Sigma}^-$ and $e^+e^- \to \Sigma^-\bar{\Sigma}^+$ with a data sample of 329.7 pb⁻¹ collected at BESIII with c.m. energies between 2.3864 and 3.0200 GeV [33]. The threshold energies for $\Sigma^+\bar{\Sigma}^-$ and $\Sigma^-\bar{\Sigma}^+$ pair production are 2.3787 GeV and 2.3949 GeV, respectively. The BESIII detector is described in detail in Ref. [34]. The critical elements for the measurements reported here are: the main drift chamber (MDC), which measures the momenta of charged particles with 0.5% resolution for 1 GeV/c tracks and the dE/dx for charged-particle identification (PID); a barrel array of scintillation counters that measures charged particles' time of flight for additional PID information; and an electromagnetic calorimeter (EMC) comprising an array of CsI(Tl) crystals that measures photon energies with a resolution of 2.5% at 1 GeV.

Simulated event samples produced with a GEANT4-based [35] Monte Carlo (MC) package that includes the geometric description of the BESIII detector and its response, are used to determine the detection efficiency and to estimate the backgrounds. The signal processes $e^+e^- \to \Sigma^{\pm}\bar{\Sigma}^{\mp}$ are generated according to the differential amplitude presented in Ref. [36]. Initial state radiation (ISR) is simulated with CONEXC [37] and the corresponding correction factors are calculated for higher order processes. Background from the QED processes $e^+e^- \to l^+l^-$ ($l = e, \mu$) and $e^+e^- \to \gamma\gamma$ are investigated with BABAYAGA [38], while for $e^+e^- \to$ hadrons and two-photon processes we use LUNDARLW [39] and BESTWOGAM [40], respectively.

3. Data analysis

In the process $e^+e^- \to \Sigma^+\bar{\Sigma}^-$, there are four dominant final state topologies which account for more than 99% of its total decay width: $p\pi^0\bar{p}\pi^0$, $n\pi^+\bar{p}\pi^0$, $p\pi^0\bar{n}\pi^-$ and $n\pi^+\bar{n}\pi^-$. All four configurations are selected in this analysis, significantly improving the statistics. At BESIII, charged particles are efficiently detected and identified by the MDC and PID systems and π^0 mesons are reconstructed in the EMC via their $\pi^0 \to \gamma\gamma$ decay mode. The selection criteria for charged tracks, PID, and photon candidates are the same as those used in Ref. [41]. Most of the anti-neutrons ($\bar{n}$) annihilate in the EMC and produce several secondary particles with a total energy deposition that can be as high as 2 GeV; the position of the $\bar{n}$ interaction and, from this, the $\bar{n}$ direction can be inferred from the weighted center-of-energy of the shower [17]. Neutron (n) detection is not done because of its low interaction efficiency and small energy deposition.

The $p\pi^0\bar{p}\pi^0$ and $n\pi^+\bar{p}\pi^0$ final-state configurations, classified as category A, can be analyzed by a partial reconstruction technique in which only the detection of $\bar{\Sigma}^- \to \bar{p}\pi^0$ is required. Candidate events are required to have at least one charged track that is identified as a $\bar{p}$ by the PID system and at least two good photons that are consistent with originating from $\pi^0 \to$
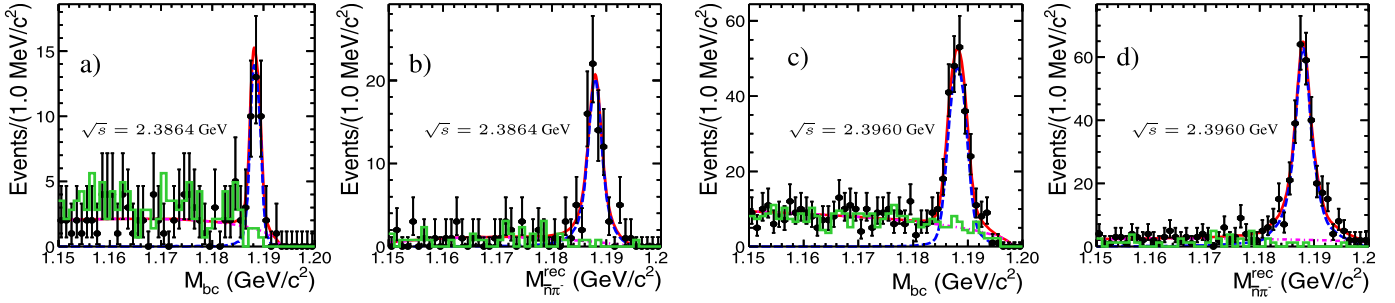
Fig. 1. The mass spectra of M_{bc} (category A) and $M_{\bar{n}\pi^-}^{rec}$ (category B) for $e^+e^- \to \Sigma^+\bar{\Sigma}^-$ candidate events at a,b) $\sqrt{s} = 2.3864$ GeV. Dots with error bars are the data; histograms are the background events in MC samples after normalization. Solid curves are the fit results, dashed curves are the signal, and dot-dashed curves are the background.

$\gamma\gamma$. The mass spectrum of $\gamma\gamma$ is required to be from $0.127 < M_{\gamma\gamma} < 0.139$ GeV/c^2 to $0.123 < M_{\gamma\gamma} < 0.14$ GeV/c^2, depending on c.m. energies. The $\bar{\Sigma}^-$ is reconstructed using all combinations of the selected $\bar{p}\gamma\gamma$. The two-body process exploits two variables that are based on energy and momentum conservation: the energy difference $\Delta E \equiv E - E_{beam}$ and the beam-constrained mass $M_{bc} \equiv \sqrt{E_{beam}^2 - p^2}$. Here, $E(p)$ is the total measurement energy (momentum) of the $\bar{p}\gamma\gamma$ combinations in the c.m. system, and E_{beam} is the beam energy. Candidates are accepted with optimized ΔE requirements of $-16 < \Delta E < 7$ MeV to $-24 < \Delta E < 13$ MeV, depending on c.m. energies, and with $M_{bc} > 1.15$ GeV/c^2.

The $p\pi^0\bar{n}\pi^-$ and $n\pi^+\bar{n}\pi^-$ final states, classified as category B, are reconstructed by requiring two good charged tracks with one identified as a π^- and the other identified as either a π^+ or p, and the most energetic shower in these events is assigned as the $\bar{n}$ candidate. To discriminate $\bar{n}$-initiated showers from those produced by photons, three variables are retained for further selection based on c.m. energy-dependent requirements: the total energy in the $\bar{n}$-assigned EMC shower, the second moment of the shower [17], and the number of crystals with above-threshold signals within a $40°$ cone around the shower. After that, kinematic fits that include the $\bar{n}$ direction are performed to identify signal events. Since the $\bar{n}$ shower does not provide a good measure of its total energy, $E_{\bar{n}}$, this is left as a free parameter in the kinematic fits. If a π^+ is identified, the fit imposes the $n\bar{n}\pi^+\pi^-$ hypothesis with a missing n. If a p is identified, the fit imposes the $p\bar{n}\pi^-\pi^0$ hypothesis with a missing π^0. In both fits, total energy-momentum conservation is constrained and $M_{\bar{n}\pi^-}$ is also constrained to the mass of the $\bar{\Sigma}^-$. The $p\pi^-$ invariant mass is required to be $|M(p\pi^-) - m(\Lambda)| > 0.005$ GeV/c^2 to eliminate background from $e^+e^- \to \Lambda\bar{\Lambda} \to p\pi^-\bar{n}\pi^0$. Furthermore, the χ^2 value from the kinematic fit is required to be less than 20.

The reconstruction of $e^+e^- \to \Sigma^-\bar{\Sigma}^+$ is similar to that for $n\pi^+\bar{n}\pi^-$ in the $e^+e^- \to \Sigma^+\bar{\Sigma}^-$ analysis since they have the same final states. The only difference is that $M_{\bar{n}\pi^+}$ is constrained to the mass of the $\bar{\Sigma}^+$ in the kinematic fit.

Fig. 1 shows the distributions of M_{bc} for category A and the recoil mass of $\bar{n}\pi^-$, $M_{\bar{n}\pi^-}^{rec}$, for category B using selected $e^+e^- \to \Sigma^+\bar{\Sigma}^-$ candidates, where significant signals in both categories are observed in data at $\sqrt{s} = 2.3864$ and 2.3960 GeV. Backgrounds are studied with MC samples and only hadronic final states survive the selection criteria. In category A, the backgrounds are from e^+e^- annihilation events with the same final states as the signal process, with one or more additional π^0, and with an additional γ-ray. In category B, the backgrounds are from annihilation events with the same final states as the signal process, multi-π processes such as $\pi^+\pi^-\pi^0\pi^0$ and processes with one more π^0 in the final states. These background processes are mainly from contributions including intermediate states such as Δ, Λ and Σ baryons, but none of them produce peaks in the signal regions as shown by
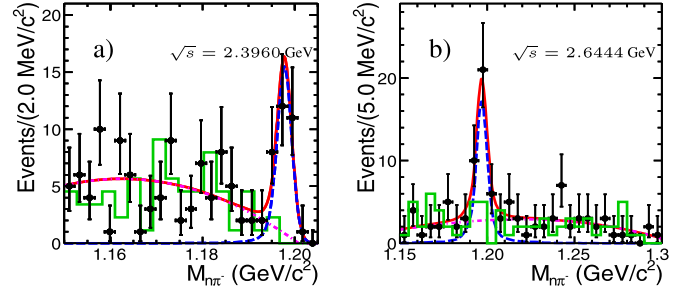
Fig. 2. The $M_{n\pi^-}$ distributions for selected $e^+e^- \to \Sigma^-\bar{\Sigma}^+$ events at a) $\sqrt{s} = 2.3960$ GeV and b) $\sqrt{s} = 2.6444$ GeV. Dots with error bars are the data; histograms are the background events in MC after normalization. Solid curves are the fit results, dashed curves are the signal, and dot-dashed curves are the background.

the histograms of Fig. 1. Fig. 2 shows distributions of $M_{n\pi^-}$ for $e^+e^- \to \Sigma^-\bar{\Sigma}^+$ candidate events at $\sqrt{s} = 2.3960$ and 2.6444 GeV, respectively, where significant signals in data are observed. In the background study, no peaking background is observed in the $n\pi^-$ mass spectrum.

The Born cross section for $e^+e^- \to \Sigma^+\bar{\Sigma}^-$ is determined from the relation:

$$\sigma^B = \frac{N_i}{\mathcal{L}(1+\delta^r)\frac{1}{|1-\Pi|^2}\delta_i^{data/MC}\mathcal{B}_i\varepsilon_i}, \quad (i = A, B), \tag{2}$$

where N is the signal yield extracted from the fits; $\mathcal{L}$ is the integrated luminosity; $1+\delta^r$ is the ISR correction factor incorporating the input cross section from this analysis iteratively; $\frac{1}{|1-\Pi|^2}$ is the vacuum polarization factor [42]; ε is the detection efficiency determined from signal MC events. The factor $\delta^{data/MC}$ is a correction factor for efficiency differences between data and MC simulation, determined from studies of high statistics, low-background control samples of $J/\psi \to \Sigma^+\bar{\Sigma}^-$ and $J/\psi \to \Lambda\bar{\Sigma}^-\pi^+$, respectively. The decay branching fraction $\mathcal{B}$ accounts for the intermediate states in the $\bar{\Sigma}^-$ decay (51.57% for $\bar{\Sigma}^- \to \bar{p}\pi^0$ and 48.31% for $\bar{\Sigma}^- \to \bar{n}\pi^-$).

To determine the signal yields, un-binned maximum likelihood fits are performed to the M_{bc} and $M_{n\pi^+}$ distributions for categories A and B, respectively. The probability density function (PDF) for the signal is described with a MC-simulated shape convolved with a Gaussian function to account for mass resolution differences between data and MC simulation. The background PDF for category A is described by an Argus function [43]; for category B by a second order polynomial. In the fit, the two categories are constrained by the same Born cross section σ^{Born}, and the expected signal yields are calculated from $N_i = \sigma^{Born} \cdot \mathcal{L} \cdot \varepsilon_i \cdot (1+\delta) \cdot \delta_i^{data/MC} \cdot \mathcal{B}_i$. The fit results at $\sqrt{s} = 2.3864$ and $\sqrt{s} = 2.3960$ GeV are shown in Fig. 1. Similarly, the signal yield of $e^+e^- \to \Sigma^-\bar{\Sigma}^+$ is determined by fitting the $n\pi^-$ mass spectrum, where the signal is described with the MC simulated shape convolved with a Gaussian function

Table 1

Summary of the calculated cross section for $e^+e^- \to \Sigma^+\bar{\Sigma}^-$ and effective FFs of Σ^+ at each c.m. energy and the quantities used in the calculation, $\epsilon = \varepsilon(1+\delta^r)\frac{1}{|1-\Pi|^2}\delta^{\text{data/MC}}$, defined in the text. The energy points with asterisks are combined data samples with c.m energies weighted by the luminosities of the subsamples. The 2.7500 GeV is a combined data set of 2.7000 and 2.8000 GeV, and 2.9884 GeV is a combined data set of 2.9500, 2.9810, 3.0000 and 3.0200 GeV. The last column shows the results of $|G_E/G_M|$ ratio of Σ^+.

$\sqrt{s}$ (GeV)	$\mathcal{L}$ (pb^{-1})	ϵ_A(%)	ϵ_B(%)	σ^{Born} (pb)	$|G_{\text{eff}}|(\times 10^{-2})$	$|G_E/G_M|$
2.3864	22.6	5.8	12.6	$58.2 \pm 5.9^{+2.8}_{-2.6}$	$16.5 \pm 0.9 \pm 0.9$	-
2.3960	66.9	9.5	14.1	$68.6 \pm 3.4 \pm 2.3$	$15.0 \pm 0.4 \pm 0.5$	$1.83 \pm 0.26 \pm 0.24$
2.5000	1.10	18.4	21.6	$130 \pm 29 \pm 11$	$14.0 \pm 1.6 \pm 0.6$	–
2.6444	33.7	24.4	20.5	$59.9 \pm 3.6 \pm 3.2$	$8.6 \pm 0.3 \pm 0.2$	$0.66 \pm 0.15 \pm 0.11$
2.6464	34.0	24.2	20.7	$58.9 \pm 3.5 \pm 2.4$	$8.5 \pm 0.3 \pm 0.2$	
*2.7500	2.04	25.0	19.7	$36.9 \pm 12.8 \pm 3.2$	$6.7 \pm 1.2 \pm 0.3$	–
2.9000	105.	26.5	20.6	$16.7 \pm 1.2 \pm 1.1$	$4.5 \pm 0.2 \pm 0.2$	$1.06 \pm 0.36 \pm 0.09$
*2.9884	65.2	25.5	21.4	$12.4 \pm 1.3 \pm 1.3$	$3.9 \pm 0.2 \pm 0.2$	–

Table 2

Summary of the calculated cross section for $e^+e^- \to \Sigma^-\bar{\Sigma}^+$ and effective FFs of Σ^- at each c.m. energy and the quantities used in the calculation.

$\sqrt{s}$ (GeV)	$\mathcal{L}$ (pb^{-1})	ϵ(%)	N	σ^{Born} (pb)	$|G_{\text{eff}}|(\times 10^{-2})$
2.3864	22.6		(below threshold)		
2.3960	66.9	18.8	29.6 ± 6.7	$2.3 \pm 0.5 \pm 0.3$	$3.9 \pm 0.5 \pm 0.6$
2.5000	1.10	20.2	$4.8^{+2.9}_{-2.2}$	$21.2^{+12.7}_{-9.5} \pm 1.4$	$5.9^{+1.8}_{-1.3} \pm 0.2$
2.6444	33.7	16.7	33.1 ± 7.7	$5.8 \pm 1.4 \pm 0.4$	$2.8 \pm 0.3 \pm 0.1$
2.6464	34.0	16.8	38.0 ± 8.4	$6.6 \pm 1.5 \pm 0.5$	$2.9 \pm 0.3 \pm 0.1$
2.9000	105.	14.2	18.0 ± 7.1	$1.2 \pm 0.5 \pm 0.1$	$1.2 \pm 0.2 \pm 0.1$
*2.9884	65.2	14.9	$9.4^{+5.4}_{-4.6}$	$1.0^{+0.6}_{-0.5} \pm 0.1$	$1.1 \pm 0.3 \pm 0.1$

and the background is described with a 2nd-order polynomial. Fit results at $\sqrt{s} = 2.3960$ and $\sqrt{s} = 2.6444$ GeV are shown in Fig. 2.

The quantities used in the cross section calculations for $e^+e^- \to \Sigma^+\bar{\Sigma}^-$ and $e^+e^- \to \Sigma^-\bar{\Sigma}^+$ are summarized in Tables 1 and Table 2, respectively. It should be noted that, due to limited statistics, data at c.m energies 2.7000 and 2.8000 GeV are combined; data at 2.9500, 2.9810, 3.0000 and 3.0200 GeV are combined. Currently, individual measurements on $|G_E|$ and $|G_M|$ at each energy point are not possible due to statistics. Therefore, the effective FFs of $\Sigma^{\pm}$, defined as $|G_{\text{eff}}|^2 \equiv (|G_E|^2 + 2\tau|G_M|^2)/(2\tau + 1)$ [44], are reported here and shown in Table 1, 2.

Systematic uncertainties associated with the cross section measurements include event selection, cross section line-shape, angular distribution, fitting method, energy scale, and luminosity. In the nominal results, the differences of data and MC efficiencies are corrected with control samples. We vary the data/MC correction factors within their $\pm 1\sigma$ uncertainty and the resulting differences in the cross sections are taken as the uncertainty from the event selection. The uncertainty associated with the cross section line-shape is 1.0%, which includes both the theoretical uncertainty and the parameter uncertainty in the line-shape fit. The uncertainty from the angular distribution is evaluated by varying $|G_E/G_M|$ ratios within $\pm 1\sigma$ at the three energy points with the highest statistics. For the energy points with unknown $|G_E/G_M|$ values, two extreme cases $G_E = 0$ and $G_M = 0$ are considered and the difference in the efficiencies divided by a factor of $\sqrt{12}$ is taken as the uncertainty [45]. Alternative fits are performed to study the uncertainty from the fit procedure. These include varying the fitting range, varying the signal shape by fixing the resolution of the convolved Gaussian to be $\pm 1\sigma$ different from its nominal value, and changing the background PDF from a second order to a third order polynomial. The effects of the c.m. energy and energy resolution uncertainties are studied for energy points near threshold. The difference of the cross sections in $e^+e^- \to \Sigma^+\bar{\Sigma}^-$ is very small and the corresponding uncertainty on the cross sections can be neglected. The uncertainty on the effective FFs are 4.9% and 2.8% at $\sqrt{s} = 2.3864$ and 2.396 GeV due to the change of Coulomb correction factors. For the $e^+e^- \to \Sigma^-\bar{\Sigma}^+$ process, the variation of c.m energy and energy resolution introduce uncertainties of 12.0%

and 14.2% in the cross section and effective FF, respectively, at $\sqrt{s} = 2.396$ GeV. The integrated luminosity is determined with large angle Bhabha events with an uncertainty of 1.0% [33]. All sources of systematic uncertainties are treated as uncorrelated and summed in quadrature; they are in the range between 3.5% and 13.0% of the cross sections, depending on the c.m. energy.

4. Line shape analysis

The measured cross section line-shapes of $e^+e^- \to \Sigma^{\pm}\bar{\Sigma}^{\mp}$ from $\sqrt{s} = 2.3864$ to 3.0200 GeV are shown in Fig. 3. The near threshold cross sections for $e^+e^- \to \Sigma^+\bar{\Sigma}^-$ and $e^+e^- \to \Sigma^-\bar{\Sigma}^+$ are measured to be $58.2 \pm 5.9^{+2.8}_{-2.6}$ and $2.3 \pm 0.5 \pm 0.3$ pb, respectively, both are inconsistent with the value of 520 pb expected for point-like charged baryons. Instead, a new feature is observed in which the cross sections for $e^+e^- \to \Sigma^-\bar{\Sigma}^+$ are consistently smaller than those for $e^+e^- \to \Sigma^+\bar{\Sigma}^-$. A perturbative QCD-motivated energy power function [46,47], given by

$$\sigma^{\text{B}}(s) = \frac{\beta C}{s}\left(1 + \frac{2m_B^2}{s}\right)\frac{c_0}{(s-c_1)^4[\pi^2 + \ln^2(s/\Lambda_{\text{QCD}}^2)]^2} \quad (3)$$

is used to fit the line-shapes, where c_0 is the normalization, c_1 is the mean effect of a set of intermediate states that mediates the coupling between the virtual photon [48] and is regarded as common for the two processes, and Λ_{QCD} is the QCD scale, fixed to 0.3 GeV. The fit results are shown in Fig. 3 with a fit quality of $\chi^2/\text{ndof} = 9.7/12$, where ndof is number of degrees of freedom. The cross section ratio between $e^+e^- \to \Sigma^+\bar{\Sigma}^-$ and $e^+e^- \to \Sigma^-\bar{\Sigma}^+$ is obtained from c_0 to be 9.7 ± 1.3, and c_1 is 2.0 ± 0.2 GeV^2. Since the effective FF is proportional to the square root of the Born cross section, the ratio of the effective Σ^+ and Σ^- FFs is consistent with 3, which is the ratio of the incoherent sum of the squared charges of the Σ^+ and Σ^- valence quarks, $\sum_{q\in B} Q_q^2$.

The results are in disagreement with the prediction from octet baryon wave functions [22], where the typical $SU(3)$-symmetry breaking effects for hyperon FFs are about $10 \sim 30\%$. In the diquark model, the Σ^+ FFs should be comparable to that of Λ [23].
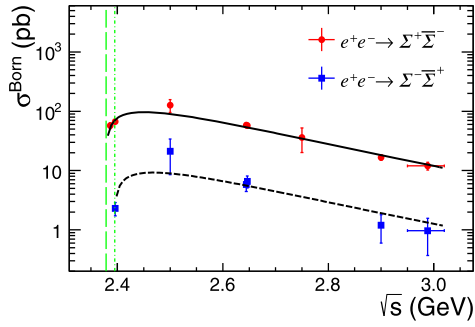
Fig. 3. The cross section lineshapes for $e^+e^- \to \Sigma^+\bar{\Sigma}^-$ (circles) and $e^+e^- \to \Sigma^-\bar{\Sigma}^+$ (squares). The solid line is the pQCD fit for $e^+e^- \to \Sigma^+\bar{\Sigma}^-$ and the dashed line for $e^+e^- \to \Sigma^-\bar{\Sigma}^+$. The vertical dashed and dotted lines denote production thresholds for $e^+e^- \to \Sigma^+\bar{\Sigma}^-$ and $e^+e^- \to \Sigma^-\bar{\Sigma}^+$.
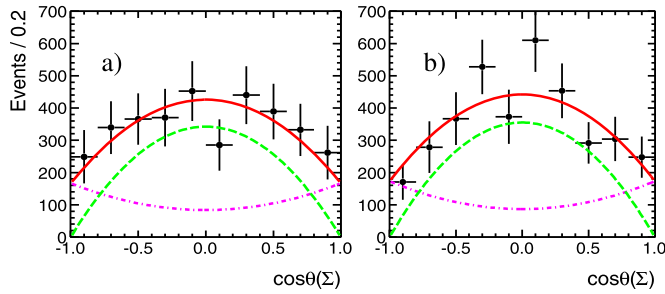
Fig. 4. Simultaneous fit of efficiency corrected angular distribution at $\sqrt{s} = 2.396$ GeV for a) category A b) category B for $e^+e^- \to \Sigma^+\bar{\Sigma}^-$ events. Dots with error bars are data, solid curves are the fit results, the contributions from G_E and G_M are indicated by dashed and dotted curves.

The $\Sigma^\pm$ FFs are also predicted in Ref. [24] from Unitary and Analytic model. We notice that a recent prediction for the non-resonant cross section of $e^+e^- \to \Sigma^\pm\bar{\Sigma}^\mp$ at the J/ψ mass [49], based on an effective Lagrangian density, is consistent with our result when extrapolated to $\sqrt{s} = 3.097$ GeV using Eq. (3).

5. Extraction of $|G_E/G_M|$ ratio

The value of $|G_E/G_M|$ can be obtained by fitting the differential angular distribution according to Eq. (1). The statistics at $\sqrt{s} = 2.3960, 2.6444, 2.6464$ and 2.9000 GeV for $e^+e^- \to \Sigma^+\bar{\Sigma}^-$ allow us to perform a study of the polar angle of Σ^+ in the c.m. frame. The angular distributions for categories A and B at $\sqrt{s} = 2.3960$ GeV are shown in Fig. 4. These angular distributions have been corrected for the detection efficiency and ISR, which are obtained from signal MC simulation. Additional bin-by-bin corrections due to the data/MC detection differences, for categories A and B, respectively, have also been applied. Simultaneous fits to the two data sets to the expression in Eq. (1) sharing a common value for $|G_E/G_M|$ are performed. The result of $|G_E/G_M| = 1.83 \pm 0.26$ is significantly higher than 1. Using the normalized number of events, $|G_M|$ is determined to be $(9.14 \pm 1.42) \times 10^{-2}$ and $(9.30 \pm 1.53) \times 10^{-2}$ for category A and B, respectively. Similar angular distribution fits are performed for the combined $\sqrt{s} = 2.6444$ and 2.6464 GeV data sets, denoted as 2.6454 GeV, and $\sqrt{s} = 2.90$ GeV and the results are listed in Table 1. The systematic uncertainties on $|G_E/G_M|$ considered here are the difference between data and MC efficiency, the bin size, and the fit range. For the Σ^-, on the other hand, the statistics only allow for the determination of $|G_{\text{eff}}|$; they are not sufficient to extract $|G_E/G_M|$.

6. Summary

In summary, the data collected by BESIII at c.m. energies between 2.3864 and 3.0200 GeV, are exploited to perform measurements of $e^+e^- \to \Sigma^\pm\bar{\Sigma}^\mp$. This is the first time that cross sections of $e^+e^- \to \Sigma^\pm\bar{\Sigma}^\mp$ in the off-resonance region are presented. The precision has been significantly improved by reconstructing all dominant decay modes of the Σ. Cross sections near threshold are observed for $e^+e^- \to \Sigma^+\bar{\Sigma}^-$ and $e^+e^- \to \Sigma^-\bar{\Sigma}^+$ to be $58.2 \pm 5.9^{+2.8}_{-2.6}$ and $2.3 \pm 0.5 \pm 0.3$ pb, respectively. The values disagree with the point-like expectations near threshold, $848(m_p/m_B)^2$ pb, as has been seen for the proton [12,13]. The cross section line-shapes for $e^+e^- \to \Sigma^+\bar{\Sigma}^-$ and $e^+e^- \to \Sigma^-\bar{\Sigma}^+$ are well-described by pQCD-motivated functions. The ratio of the $\sigma^{\text{Born}}(e^+e^- \to \Sigma^+\bar{\Sigma}^-)$ to $\sigma^{\text{Born}}(e^+e^- \to \Sigma^-\bar{\Sigma}^+)$ is determined to be 9.7 ± 1.3, which is inconsistent with predictions from various models [22–24]. The EMFF ratio $|G_E/G_M|$ of the Σ^+ is determined from its production angle dependence at three high-statistics energy points. The $|G_E/G_M|$ of the Σ^+ shows similar features to those of the proton [12,14], Λ [18], and Λ_c [29], that is larger than 1 within uncertainties near threshold and consistent with 1 at higher c.m. energies.

Declaration of competing interest

The authors declare that they have no known competing financial interests or personal relationships that could have appeared to influence the work reported in this paper.

Acknowledgements

References

[1] R. Frisch, O. Stern, Z. Phys. 85 (1933) 4.
[2] R. Hofstadter, Rev. Mod. Phys. 28 (1956) 214.
[3] J.C. Bernauer, et al., Phys. Rev. Lett. 105 (2010) 242001;
R. Pohl, et al., Nature 466 (2010) 213;
N. Bezginov, et al., Science 365 (6457) (2019) 1007.

[4] G. Eichmann, H. Sanchis-Alepuz, R. Williams, R. Alkofer, C.S. Fischer, Prog. Part. Nucl. Phys. 91 (2016) 1.

[5] G. Ramalho, K. Tsushima, A.W. Thomas, J. Phys. G 40 (2013) 015102;
F. Gross, G. Ramalho, K. Tsushima, Phys. Lett. B 690 (2010) 183.

[6] L.S. Geng, J. Martin Camalich, L. Alvarez-Ruso, M.J. Vicente Vacas, Phys. Rev. Lett. 101 (2008) 222002.

[7] S.J. Brodsky, G.R. Farrar, Phys. Rev. D 11 (1975) 1309.

[8] J.R. Green, J.W. Negele, A.V. Pochinsky, S.N. Syritsyn, M. Engelhardt, S. Krieg, Phys. Rev. D 90 (2014) 074507.

[9] I.A. Qattan, et al., Phys. Rev. Lett. 94 (2005) 142301.

[10] A.J.R. Puckett, et al., Phys. Rev. C 85 (2012) 045203.

[11] T.K. Pedlar, et al., CLEO Collaboration, Phys. Rev. Lett. 95 (2005) 261803.

[12] J.P. Lees, et al., BaBar Collaboration, Phys. Rev. D 87 (2013) 092005.

[13] R.R. Akhmetshin, et al., CMD-3 Collaboration, Phys. Lett. B 759 (2016) 634.

[14] M. Ablikim, et al., BESIII Collaboration, Phys. Rev. Lett. 124 (2020) 042001.

[15] B. Aubert, et al., BaBar Collaboration, Phys. Rev. D 76 (2007) 092006.

[16] S. Dobbs, K.K. Seth, A. Tomaradze, T. Xiao, G. Bonvicini, Phys. Rev. D 96 (2017) 092004.

[17] M. Ablikim, et al., BESIII Collaboration, Phys. Rev. D 97 (2018) 032013.

[18] M. Ablikim, et al., BESIII Collaboration, Phys. Rev. Lett. 123 (2019) 122003.

[19] A. Antonelli, et al., Nucl. Phys. B 517 (1998) 3.

[20] S. Ahmed for the BESIII Collaboration, New features of the neutron electromagnetic structure in the electron-positron annihilation, Alberta, Canada, 2020, Feb. 9–15, talk at Lake Louise Winter Institute.

[21] J.R. Ellis, M. Karliner, New J. Phys. 4 (2002) 18.

[22] V.L. Chernyak, A.R. Zhitnitsky, Phys. Rep. 112 (1984) 173;
V.L. Chernyak, A.A. Ogloblin, I.R. Zhitnitsky, Z. Phys. C 42 (1989) 569.

[23] M. Anselmino, et al., Rev. Mod. Phys. 65 (1993) 1199;
R.L. Jaffe, F. Wilczek, Phys. Rev. Lett. 91 (2003) 232003;
R.L. Jaffe, Phys. Rep. 409 (2005) 1.

[24] G. Ramalho, M.T. Pena, K. Tsushima, Phys. Rev. D 101 (2020) 014014.

[25] N. Cabibbo, R. Gatto, Phys. Rev. 124 (1961) 1577.

[26] J. Schwinger, Particle, Sources, and Field, vol. 3, Perseus Books Publishing, Massachusetts, 1998.

[27] A.B. Arbuzov, T.V. Kopylova, J. High Energy Phys. 1204 (2012) 009.

[28] P.A. Zyla, et al., Particle Data Group, Prog. Theor. Exp. Phys. 2020 (2020) 083C01.

[29] M. Ablikim, et al., BESIII Collaboration, Phys. Rev. Lett. 120 (2018) 132001.

[30] L.Y. Dai, J. Haidenbauer, U.G. Meissner, Phys. Rev. D 96 (2017) 116001.

[31] B. El-Bennich, M. Lacombe, B. Loiseau, S. Wycech, Phys. Rev. C 79 (2009) 054001.

[32] R. Baldini Ferroli, S. Pacetti, A. Zallo, A. Zichichi, Eur. Phys. J. A 39 (2009) 315;
R. Baldini Ferroli, S. Pacetti, A. Zallo, Eur. Phys. J. A 48 (2012) 33.

[33] M. Ablikim, et al., BESIII Collaboration, Chin. Phys. C 41 (2017) 063001.

[34] M. Ablikim, et al., BESIII Collaboration, Nucl. Instrum. Methods A 614 (2010) 345.

[35] S. Agostinelli, et al., GEANT4 Collaboration, Nucl. Instrum. Methods A 506 (2003) 250.

[36] G. Fäldt, Eur. Phys. J. A 51 (2015) 74;
G. Fäldt, Eur. Phys. J. A 52 (2016) 141.

[37] R.G. Ping, Chin. Phys. C 38 (2014) 083001.

[38] G. Balossini, et al., Nucl. Phys. B 758 (2006) 227;
G. Balossini, et al., Phys. Lett. B 663 (2008) 209.

[39] B. Andersson, H. Hu, arXiv:hep-ph/9910285.

[40] S. Nova, A. Olchevski, T. Todorov, 1990, DELPHI-90-35 PROG 152;
S. Nova, A. Olchevski, T. Todorov, DELPHI Collaboration, 1990, DELPHI 90-35 PROG 152.

[41] M. Ablikim, et al., BESIII Collaboration, Phys. Rev. D 101 (2020) 092002.

[42] S. Actis, et al., Working Group on Radiative Corrections and Monte Carlo Generators for Low Energies, Eur. Phys. J. C 66 (2010) 585.

[43] H. Albrecht, et al., ARGUS Collaboration, Phys. Lett. B 241 (1990) 278.

[44] M. Ablikim, et al., BESIII Collaboration, Phys. Rev. D 91 (2015) 112004.

[45] R. Wanke, Systematic Uncertainties, Terascale Statistics Tools School, DESY, Mar 21, 2015-p. 1/56.

[46] S. Pacetti, R. Baldini Ferroli, E. Tomasi Gustafsson, Phys. Rep. 550–551 (2015) 1.

[47] G.P. Lepage, S.J. Brodsky, Phys. Rev. D 22 (1980) 2157.

[48] H.W. Hammer, U.G. Meissner, D. Drechsel, Phys. Lett. B 385 (1996) 343.

[49] R. Baldini Ferroli, A. Mangoni, S. Pacetti, K. Zhu, Phys. Lett. B 799 (2019) 135041.